Structural and optical properties of TiO_2 thin films prepared by spin coating

How to cite:

I. Sta, M. Jlassi, M. Hajji, M.F. Boujmil, R. Jerbi, M. Kandyla, M. Kompitsas, and H. Ezzaouia, Structural and optical properties of TiO_2 thin films prepared by spin coating, Journal of Sol-Gel Science and Technology 72, 421 (2014).

Structural and optical properties of TiO_2 thin films prepared by spin coating

I.Sta[*1], M.Jlassi[1], M.Hajji[1,2], M.F. Boujmil[1],R. Jerbi[1], M.Kandyla[3], M. Kompitsas[3] and H.Ezzaouia[1]

[1]*Photovoltaic Laboratory, Research and Technology Centre of Energy, Borj-Cedria Science and Technology Park, BP 95, 2050 Hammam-Lif, Tunisia.*

[2]*Ecole Nationale d'Electronique et des Communications de Sfax, Technopole de Sfax, BP 1163, CP 3021, Tunisia.*

[3]*National Hellenic Research Foundation, Theoretical and Physical Chemistry Institute, 48, Vasileos Konstantinou Ave., 11635 Athens, Greece*

*Email of corresponding author: imenstalpv@yahoo.fr

Abstract

Transparent semiconducting thin films of titanium oxide (TiO_2) were deposited on glass substrates by the sol–gel method and spin-coating technique. The physical properties of the prepared films were studied as a function of the number of spun-cast layers. The microstructure and surface morphology of the TiO_2 films were characterized by X-ray diffraction (XRD) and atomic force microscopy (AFM), with respect to the film thickness. The XRD analysis reveals that the films are polycrystalline with an anatase crystal structure and a preferred grain orientation in the (101) direction. The morphological properties were investigated by AFM, which shows a porous morphology structure for the films. The optical properties of the films were characterized by UV-visible spectrophotometry, which shows that the films are highly transparent in the visible region and their transparency is slightly influenced by the film thickness, with an average value above 80%. The dependence of the refractive index (n), extinction coefficient (k), and absorption coefficient (α) of the films on

the wavelength was investigated. A shift in the optical band gap energy of the films from 3.75 to 3.54 eV, as a function of the film thickness, has been observed.

Key words: *thin films; sol gel, titanium oxide; physical properties; nanomaterials.*

1. Introduction

Titanium oxide (TiO_2) thin films have attracted much attention due to their optical, physical, chemical, and electronic properties, including excellent transmittance of visible light, photocatalytic activity, high dielectric constant, high refractive index, and high chemical stability [1–3]. These properties strongly depend on the micro-/nano-structure and crystallinity of TiO_2. A variety of TiO_2 films have been developed for several applications, such as solar cells [4], photocatalysis [5,6], gas sensors [7], and antireflective coatings [8]. It is well known that TiO_2 is a n-type semiconductor with a wide indirect energy band gap [9,10]. TiO_2 generally crystallizes in three structures, the tetrahedral anatase structure (space group $I4_1/amd$, density = 3.894 g/cm^2), the rutile structure (space group P42/mnm, density = 4.25 g/cm^2), and the orthorhombic brookite structure (space group Pcab, density = 4.12 g/cm^2). The anatase and rutile structures belong to different space groups but both have a tetragonal crystal lattice. Rutile is the most stable form of TiO_2, whereas anatase and brookite are metastable and transform to the rutile phase upon heating [11–15]. The phase transformation from anatase to rutile structure depends on the growth process of the films, which is likely to be affected by defect concentration, grain boundary concentration, and particle packing [16, 17]. The characteristics of TiO_2 films depend on their crystal structure, orientation, and morphology, therefore control of the phase structure of the films during growth is important.

Various techniques have been used for the deposition of TiO_2 films, such as sol–gel deposition [18-20], spray pyrolysis [21], pulsed laser deposition [22], e-beam evaporation [23], chemical vapor deposition [24], and reactive magnetron sputtering [25]. The sol–gel

process has many advantages, such as large-area coating, low-temperature processing, controllable film morphology (porous or dense film), composition control, and low cost, therefore it is one of the most important techniques for the preparation of functional TiO_2 films. The characteristics of sol–gel deposited TiO_2 thin films may be controlled by the sol–gel processing conditions, including the choice of solvent, the solvent concentration, and the post-deposition heat treatment [26]. It is remarkable that a TiO_2 film, obtained by annealing at 400 – 700 °C, showed a predominantly anatase phase structure, which could change with the number of coatings [27]. This work aims at investigating the characteristics of TiO_2 thin films that were synthesized by the sol–gel method and post-annealed at 600 °C under ambient atmosphere. We evaluate the effect of the film thickness on their structural, morphological, optical, and electrical properties.

2. Experimental

2.1 Preparation of TiO_2 thin films

The TiO_2 sol was prepared using titanium (IV) isopropoxide ($C_{12}H_{28}O_4Ti$), 2-methoxyethanol ($C_3H_8O_2$) (99.8%, Sigma Aldrich), and diethanolamine (MEA) (99%, Merck) as the solute, solvent, and sol stabilizer, respectively. Titanium (IV) isopropoxide was first dissolved in 2-methoxyethanol, and then the resulting solution was magnetically stirred at 80°C. At the same time, MEA was added to the solution drop by drop. The molar ratio of MEA to titanium (IV) isopropoxide was kept at 1.0. After 1 h, a transparent TiO_2 sol was formed. In the sol, the titanium concentration was 0.5 mol/L. The TiO_2 sol was aged for 24 hours at room temperature. Before deposition, glass substrates were successively cleaned with acetone, ethanol, and deionized water in an ultrasonic bath. TiO_2 thin films were deposited on the glass substrates by spin coating at room temperature, with a rate of 3000 rpm for 30 s. After each spin-coating step, the films were heated on a hot plate at 300 °C in air for 15 min to remove organic contaminations. The procedure from coating to drying was repeated six times, in

order to increase the thickness of the films. All samples were post-annealed in air at 600 °C for 1 h.

2.2 Characterization

The crystallographic structure of the films was studied by X-ray diffraction (XRD), using a Bruker D 8 advance X-ray diffractometer with Cu K_{α} (k = 1.5418 Å) radiation, for 2 θ values in the range of 10 – 90°. The surface morphology of the films was characterized via atomic force microscopy (AFM) in tapping mode configuration by a Nanoscope III microscope. The optical transmittance, *T*, and reflectance, *R*, of the films were measured by a UV–vis–NIR (Lambda 950) spectrophotometer, equipped with an integrating sphere, in the wavelength range 400 – 2500 nm. The transmittance and reflectance measurements were used to calculate the refractive index and the film thickness, via the Manifacier equation [28]. The electrical resistivity was measured by a S302-X Stand alone in a four point probe configuration. All measurements were carried out at room temperature.

3. Results and discussion

3.1. Dependence of the structural properties of TiO_2 thin films on thickness

Figure 1 shows the XRD patterns of TiO_2 films with different numbers of layers. The identified peaks are (101), (112), and (211) peaks. All the peaks correspond to the tetragonal anatase phase of TiO_2 with a space group $I4_1/amd$ (JCPDS78-2486) and a preferred grain orientation in the (101) direction. The crystallite sizes are estimated by applying Scherer's equation to the major peaks of the diffraction patterns and taking an average [29]:

$$< D >= \frac{K\,\lambda}{\beta\, cos\theta} \qquad (1),$$

where *D* is the average crystallite size in angstroms (Å), *K* is a shape factor taken as 0.9, λ is the wavelength of X-ray radiation (CuKα = 1.5406 Å), β is the full width at half maximum (FWHM) after making the appropriate base line correction, and θ is the diffraction angle at the position of the peak maximum [30]. Figure 3 shows the crystallite size of the films as a

function of the number of layers. We notice that the crystallite size decreases by increasing the number of layers, and therefore the film thickness. The decrease of the crystallite size can be attributed to the nucleation process, due to the difference in the density of nucleation centers in films with different thicknesses. An increased density of nucleation centers leads to the formation of crystallites with smaller size.

3.2. Dependence of the morphological properties of TiO_2 thin films on thickness

The TiO_2 thin films prepared in this work were characterized in terms of their porosity. Figures 2(a) and 2(b) show typical AFM images of two films with one and six layers, respectively. We observe that the surface morphology and roughness of the films are significantly different. The surface of the films is spongy and the porosity changes with the number of layers. The obtained average surface roughness values (RMS) for the TiO_2 samples presented in Fig. 3 are very low, indicating a smooth surface.

3.3. Dependence of the optical properties of TiO_2 thin films on thickness

Figure 4 presents the optical transmittance (T) and reflectance (R) spectra of TiO_2 thin films with different thicknesses. All samples have high transmittance in the visible range. The average transmittance ranges from 80 to 92% with the number of layers and the reflectivity is less than 30 % for all samples. As it can be seen, all spectra exhibit interference fringes. From the transmittance and reflectivity curves we can calculate the band gap and the thickness of the films, respectively.

3.3.1 Thickness calculation

The thickness of the TiO_2 films was calculated using the reflectance data (Fig. 4). The Manifacier equation was used to calculate the thickness of the films [28]:

$$d = \frac{M\,\lambda_1\lambda_2}{2[n(\lambda_1)\lambda_2 - n(\lambda_2)\lambda_1]} \qquad (2),$$

where M is the number of oscillations between two extremes of the reflectance (M = 1 between two consecutive maxima or minima), λ_1, $n(\lambda_1)$ and λ_2, $n(\lambda_2)$ are the corresponding wavelengths and indices of refraction at the reflectance extremes. The calculated thickness of the films is shown in Fig. 7, where we can see that the thickness increases linearly with the number of deposited layers.

3.3.2 Optical band gap calculation

As shown in Fig. 4, the films are transparent (over 83%) in the visible range with a sharp absorption edge at ~350 nm. From the optical transmittance measurements we may calculate the absorption coefficient of the films, α. The absorption coefficient is mainly influenced by two factors (i) fundamental absorption and (ii) scattering losses. At shorter wavelengths, close to the absorption edge, the contribution of the scattering losses is negligible compared to that of fundamental absorption and the absorption coefficient is given by the equation [31]:

$$\alpha = \frac{\ln(100/T)}{d} \qquad (3),$$

In the high absorption region ($\alpha > 10^4$ cm^{-1}), the optical band gap energy may be determined by Tauc's relation [32]:

$$\alpha = \frac{B(\mathrm{h\nu} - \mathrm{Eg})^2}{\mathrm{h\nu}} \qquad (4),$$

where $h\nu$ is the incident photon energy, E_g the optical band gap energy, and B is a constant. Determination of the band gap energy, E_g, and its correlation with structural features are often necessary to understand the performance of a thin-film material. We evaluated the band gap energy of the TiO_2 films from $(\alpha h\nu)^{1/2}$ versus photon energy, $h\nu$, plots (not shown here), in accordance with Eq (3). For this, the plotted data have been fitted with a straight line and the regression of each linear fit was better than 0.999. E_g was estimated from the intercept of these linear fits with the photon energy axis. The optical band gap energy of the films is shown in Fig. 5. The optical band gap is found to be between 3.75 - 3.54 eV, near the value of 3.85 eV, found by H. Oh *et al.* for TiO_x with a thickness of 38 nm [33]. The optical band gap

energy decreases with the film thickness. The decrease of the band gap cannot be due to the change of the crystallite size, since the latter decreases with the film thickness, but rather to oxygen defect band states formed in the band gap. The values of the optical band gap energy are in good agreement with those published by other authors [34,35]. However, they are still higher than the optimum range for solar energy conversion.

3.3.3 Calculation of the Urbach energy

The variation of the absorption coefficient with the Urbach energy is given by the following equation [36]:

$$\alpha = \alpha_0 \exp\left(\frac{h\nu}{E_u}\right) \qquad (5),$$

where α_0 is a constant and E_u is the Urbach energy.

We calculated the Urbach energy for the TiO_2 films from the plots of Ln(α) *vs.* $h\nu$. The value of E_u is calculated from the slope of the linear region of these curves. Fig. 5 shows the value of E_u as a function of the film thickness. The obtained values of E_u are in the range of amorphous semiconductors (between 0.046 and 0.66 eV), as reported by Davis and Mott [37]. The results show an increase of the Urbach energy with the TiO_2 film thickness, which suggests the possibility of long range order, locally arising from the formation of a weak crystalline phase, as it is shown from the XRD results. The increase of the Urbach energy is attributed to the increase of the density of oxygen vacancy atoms within the TiO_2 film [38, 39].

3.3.4 Calculation of the optical constants

The optical constants (refractive index, n, and extinction coefficient, k) of the TiO_2 films were determined from the following equations [40,41], via a Matlab-based program:

$$R = \frac{(n-1)^2+k^2}{(n+1)^2+k^2} \qquad (6),$$

and

$$k = \frac{\alpha\lambda}{4\pi} \qquad (7),$$

Figure 6 shows the variation of n and k as a function of wavelength, λ, in the 400 – 2500 nm range. The refractive index, n, of undoped TiO_2 thin films prepared using sol–gel [42,43], ion-assisted electron-beam evaporation [44], or plasma vapor deposition [45,46], has been previously reported to present a fast decrease in the UV region, followed by a slower decrease in the visible and IR regions of the optical spectrum. Depending on the elemental composition, film crystalline structure and density, surface roughness, *etc.*, refractive index values between 2.6 and 3.0 for λ = 300 nm and 1.9 and 2.1 for λ = 800 nm are common for TiO_2 films. A similar behavior was found for the wavelength dependence of the extinction coefficient, k, with values usually reported to vary between 0 and 0.3. The results presented in Fig. 6 agree with the results reported in the literature. Due to the amorphous structure of the films developed in this work, the value of the refractive index at λ = 632.8 nm is smaller than the characteristic value for the anatase phase of TiO_2, which is reported to be ~2.5 [47]. The increase of the refractive index of the TiO_2 films with the number of layers, shown in Fig. 6, is due to film densification and pore filling.

3.3.5 Calculation of the relative density and porosity of the thin films

The relative density, D, is a parameter which can reflect the degree of crystallization of thin films. The relative density can be calculated using the equation [48]:

$$D = \frac{n^2-1}{{n_0}^2-1} \times 100\% \qquad (8),$$

where n is the refractive index of the samples and $n_0 = 2.52$ is the refractive index of single crystal anatase TiO_2 [49]. From Fig. 7, we observe that the relative density increases with the film thickness, indicating the crystalline quality of the TiO_2 thin films gradually improves.

The porosity of the TiO_2 films is calculated using the following equation [50]:

$$\text{Porosity} = (1 - \frac{n^2 - 1}{{n_d}^2-1}) \times 100(\%) \qquad (9),$$

where n_d is the refractive index of pore-free anatase TiO_2 (n_d = 2.52 [49]), and n is the refractive index of the samples. The porosity of TiO_2 thin films with different number of layers were shown in Fig.7. We note that the porosity of the films decreases with the number of layers. This is due to film densification and pore filling in films with increasing thickness [51].

3.4. Dependence of the electrical properties of TiO_2 thin films on thickness

The electrical resistivity of the TiO_2 films was measured by the Van der Pauw method and its dependence on the number of layers is shown in Fig. 8. From this Figure, we observe that the resistivity increases with the thickness of the films. The resistivity ranges between 4.35×10^{11} Ω.cm and 2×10^{12} Ω.cm, which is similar to the resistivity values reported by Alam and Cameron [52].

Conclusions

TiO_2 thin films were prepared by the sol–gel method on glass substrates. The structural, morphological, optical, and electrical properties of the films were studied as a function of the number of layers. The X-ray diffraction patterns of the TiO_2 films reveal the existence of a TiO_2 single-phase with the anatase crystal structure. The XRD patterns consist of a (101) main peak, which is due to TiO_2 crystals that grow along the c-axis. The morphological properties of the films show a porous morphology. The density of the films increases with the number of layers, while their porosity decreases. Both the optical transmittance and film thickness increase with the number of layers. The crystallite size and optical band gap decrease with the number of layers. The decrease in the crystallite size is attributed to the difference in nucleation center densities in films with different thicknesses. The decrease in the optical band gap is attributed to the formation of a non-stoichiometric material with increased oxygen vacancies by increasing the film thickness. These oxygen vacancies also increase the Urbach energy. The refractive index of the films increases with the number of

layers, while the extinction coefficient decreases. The electric resistivity increases with the thickness of the films, ranging between 4.35×10^{11} Ω.cm and 2×10^{12} Ω.cm.

References

[1] T.L. Chen, Y. Furubayashi, Y. Hirose, T. Hitosugi, T. Shimada, T. Hasegawa, (2007) J. Phys. D: Appl. Phys. 40:5961.

[2] O.V. Sakhno, L.M. Goldenberg, J. Stumpe, T.N. Smornova, (2007) Nanotechnology 18:105704.

[3] P.D. Prajna, S.K. Mohapatra, M. Mano, (2008) J. Phys. D: Appl. Phys. 41:245103.

[4] O'Regan, Grätzel, (1991) Nature 353:737.

[5] Kitano Masaaki, Matsuoka Masaya, Ueshima Michio, Anpo Masakazu,(2007) Appl. Catal.A Gen 325:1.

[6] Š. Kment, I. Gregora, H. Kmentová, P. Novotná, Z. Hubička, J. Krýsa, P. Sajdl, A. Dejneka, M. Brunclíková, L. Jastrabík, M. Hrabovský , (2012) J Sol-Gel Sci Technol 63:294.

[7] Ibrahim A, Al-Homoudi, J.S. Thakur, R. Naik, G.W. Auner, G. Newaz, (2007) Appl. Surf. Sci.253:8607.

[8] G. San Vicente, A. Morales, M.T. Gutiérrez, (2002) Thin Solid Films. 403–404:335.

[9] M. Gräzel, Ph.D. (1989) Heterogeneous Photochemical Electron Transfer, XRC Press, Inc.

[10] N. Serpone, D. Lawless, R. Khairutdinov, (1995) J. Phys. Chem. 99:16646.

[11] Chandana Rath, P Mohanty, A C Pandey, N C Mishra, (2009) J. Phys. D: Appl. Phys. 42:205101.

[12] M. Scepanovic et al., (2009) Acta Phys. Polonica A 116.

[13] A.I. Kingon, J.P. Maris, S.K. Steiffer, (2000) Nature (London) 406:1032.

[14] W. Li, C. Ni, H. Lin, C.P. Huang, S. Ismat Shah, (2004) J. Appl. Phys. 96 (11):6663.

[15] H. Zhang, J.F. Banfield, (1999) Am. Mineral Am Mineral 1999, 84:528-535.

[16] D.J. Reidy, J.D. Holmes, M.A. Morris, (2006) J. Eur. Ceram. Soc. 26:1527.

[17] K.P. Kumar, K. Keizer, A.J. Buggraaf, T. Okubo, H. Nagamoto, (1993) J. Mater. Chem. 3:1151.

[18] K. Pomoni, A. Vomvas, CHR. Trapalis, (2008) J. Non-Cryst. Solids 354 :4448.

[19] Morozova M, Kluson P, Krysa J, Zlamal M, Solcova O, Kment S, Steck T, (2009) J Sol Gel Sci Technol 52:398.

[20] M. Morozova, P. Kluson, J. Krysa, Ch. Gwenin, O. Solcova, (2011) J Sol-Gel Sci Technol. 58:175.

[21] C. Natarajan, N. Fukunaga, G. Nogami, (1998) Thin Solid Films. 322:6.

[22] Terashima Masahiro, Inoue Narumi, Kashiwabara Shigeru, Fujimoto Ryozo, (2001) Appl. Surf. Sci. 169–170:535.

[23] Sun Lianchao, Hou Ping, (2004) Thin Solid Films, 455–456:525.

[24] Sun Hongfu, Wang Chengyu, Pang Shihong, Li Xiping, Tao Ying, Tang Huajuan, Liu Ming, (2008) J. Non-Cryst. Solids 354:1440.

[25] S. Boukrouh, R. Bensaha, S. Bourgeois, E. Finot, M.C. Marco de Lucas, (2008) Thin Solid Films 516:6353.

[26] L. Hu, T. Yoko, H. Kozuka, S. Sakka, (1992) Thin Solid Films. 219:18.

[27] P. Kajutvichyanukul, J. Ananpattarachai, S. Pongpom, (2005) Sci. Technol. Adv. Mater. 6:352.

[28] J.C. Manifacier, J. Gasiot, J.P. Fillard, (1976) Journal of Physics E: Scientific Instruments 9:1002.

[29] M.K. Singh, A. Agarwal, R. Gopal, R.K. Swarnkar, R.K. Kotnala, (2011) J. Mater. Chem. 21:11074.

[30] B.E. Warren, (1990) X-Ray Diffraction, Dover, New York. 251.

[31] R. Swanepoel, (1983) Journal of Physics E: Scientific Instruments 16 :1214–1222.

[32] J. Tauc, R. Grigorovici, A. Vancu, (1966) Phys. Status Solidi (b) 15:627.

[33] Oh H, Krantz J, Litzov I, Stubhan T, Pinna L, Brabec C J (2011) Solar Energy Materials & Solar Cells 95:2194.

[34] Teresa M, Viseu R, Isabel M, Ferreira C (1999) Vacuum 52:115.

[35] Park YR, Kim KJ (2005)Thin Solid Films. 48434.

[36] Urbach F (1953) J. Phys. Rev. 92:1324.

[37] N. Mott, E. Davis, (1979) Electronic Process in Non-Crystalline Materials, second ed., Clarendon Press, Oxford, UK.

[38] A. Abdel-Kader, A. Higazy, M. Elkholy, (1991) J. Mater. Sci.: Mater. Electron. 2:204.

[39] B. Choudhury,A.Choudhury/PhysicaE56(2014)364–371.

[40] F. Yakuphanoglu, (2006) Opt. Mater. 29:253.

[41] F. Yakuphanoglu, A. Cukurovali, I. Yilmaz, (2004) Physica B 353:210.

[42] C. Marchand, Characterisation of TiO_2 thin films and multilayer anti-reflective coatings, Horiba Jobin Yvon UVISEL Application Note, Ref. SE — 07.

[43] M. Fernández-Rodríguez, G. Ramos, F. Del Monte, D. Levy, C.G. Alvarado, A. Núñez, A. Álvarez-Herrero, (2004) Thin Solid Films 455–456:545.

[44] P. Eiamchai, P. Chindaudom, A. Pokaipisit, P. Limsuwan, (2009) Current Applied Physics 9:707.

[45] A. Amassian, P. Desjardins, L. Martinu, (2004) Thin Solid Films 447–448:40.

[46] L. J. Meng, V. Teixeira, H.N. Cui, F. Placido, Z. Xu, M.P. Dos Santos, (2006) Applied Surface Science 252 :7970.

[47] WELLS A.F, (1984) Structural Inorganic Chemistry, 5th ed., Claredon Press: Oxford.

[48] M. Ohyama, H. Kozuka, T. Yoko, (1997) Thin Solid Films 306:78.

[49] W.D. Kingery, H.K. Bowen, D.R. Uhlmann, (1976) Introduction to Ceramics, Wiley, New York.

[50] B.E. Yoldas, P.W. Partlow, (1985) Thin Solid Films 129:1.

[51] R. Mechiakh, R. Bensaha, (2006) C. R. Physique 7:464.

[52] M.J. Alam and D.C. Cameron, (2002) Journal of Sol-Gel Science and Technology 25:137.

Figure captions

Fig. 1 The X-ray diffraction patterns of TiO_2 thin films with different numbers of layers.

Fig. 2 AFM images of TiO_2 thin films with one and six layers.

Fig. 3 Crystallite size and surface roughness of TiO_2 thin films as a function of the number of layers.

Fig. 4 Transmission and reflectance spectra of TiO_2 thin films with different number of layers.

Fig. 5 The optical band gap and Urbach energy of TiO_2 thin films as a function of the number of layers.

Fig. 6 The refractive index (*n*) and extinction coefficient (*k*) of TiO_2 thin films with different numbers of layers.

Fig. 7. Thickness, porosity, and relative density of TiO_2 thin films as a function of the number of layers.

Fig. 8 Electric resistivity for TiO_2 thin films as a function of the number of layers.

Figure 1

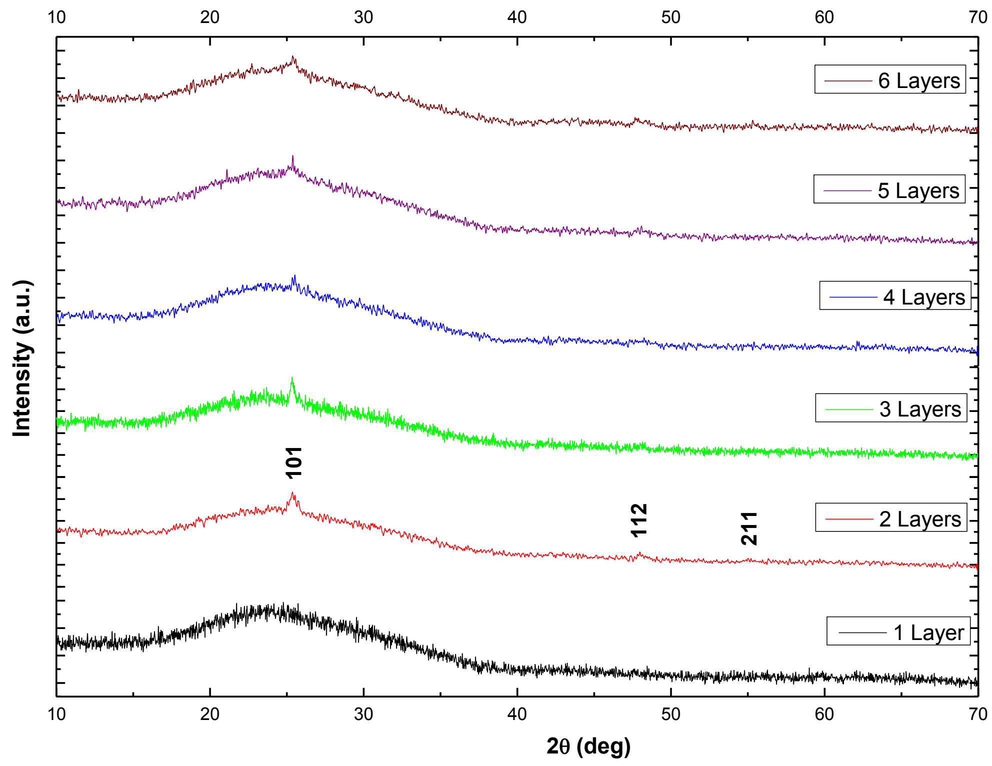

Figure 2

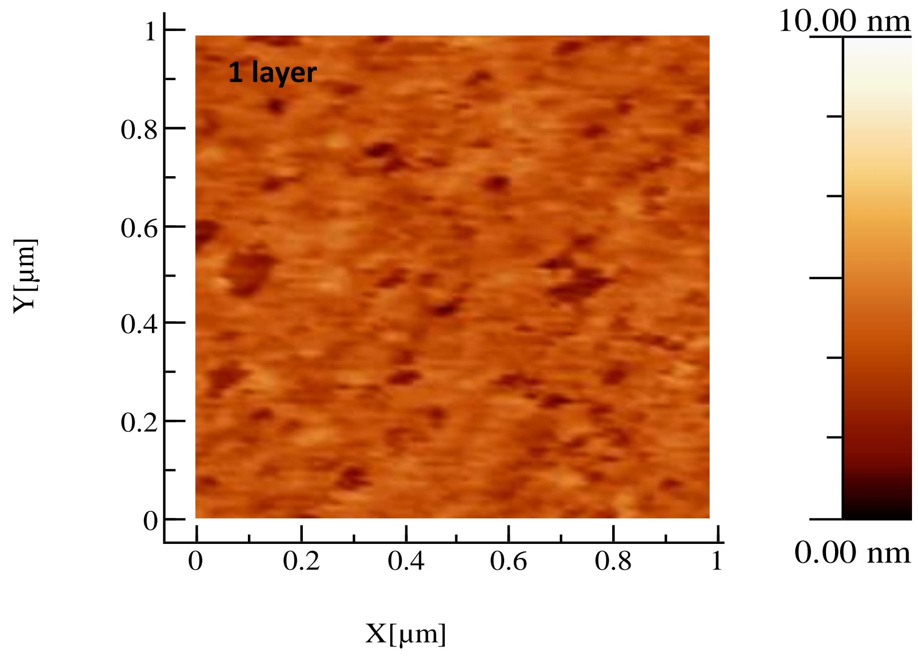

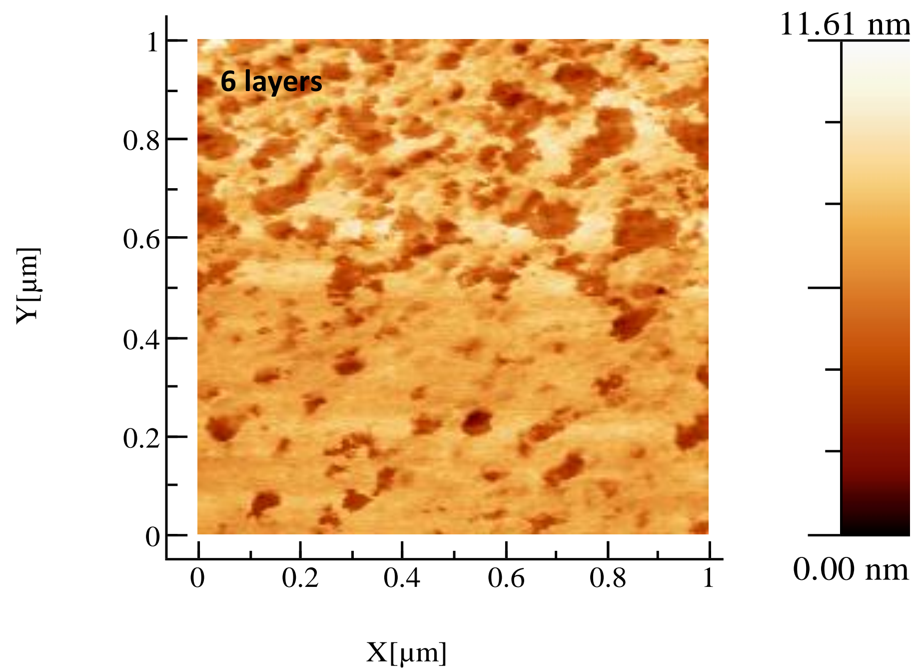

Figure 3

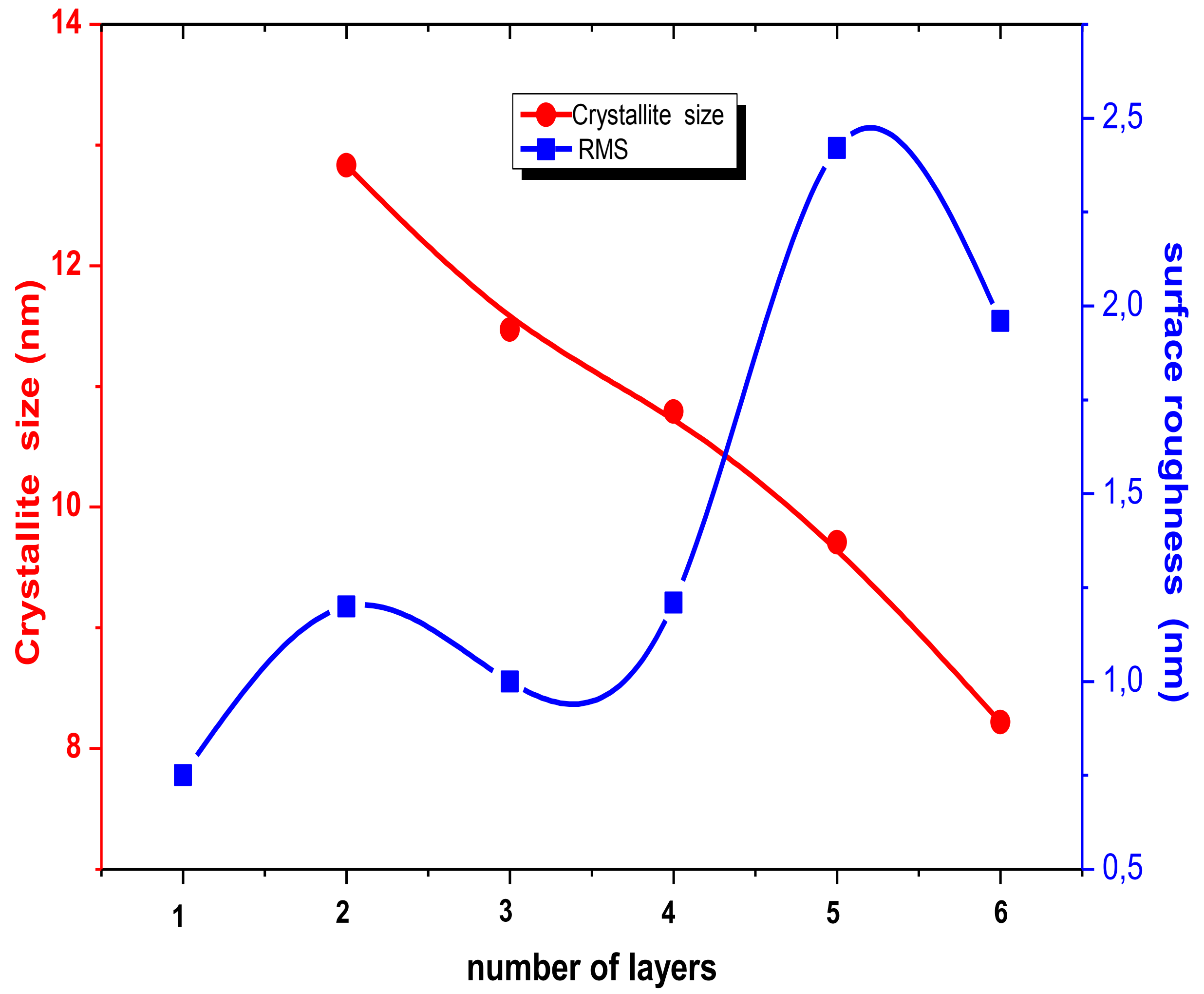

Figure 4

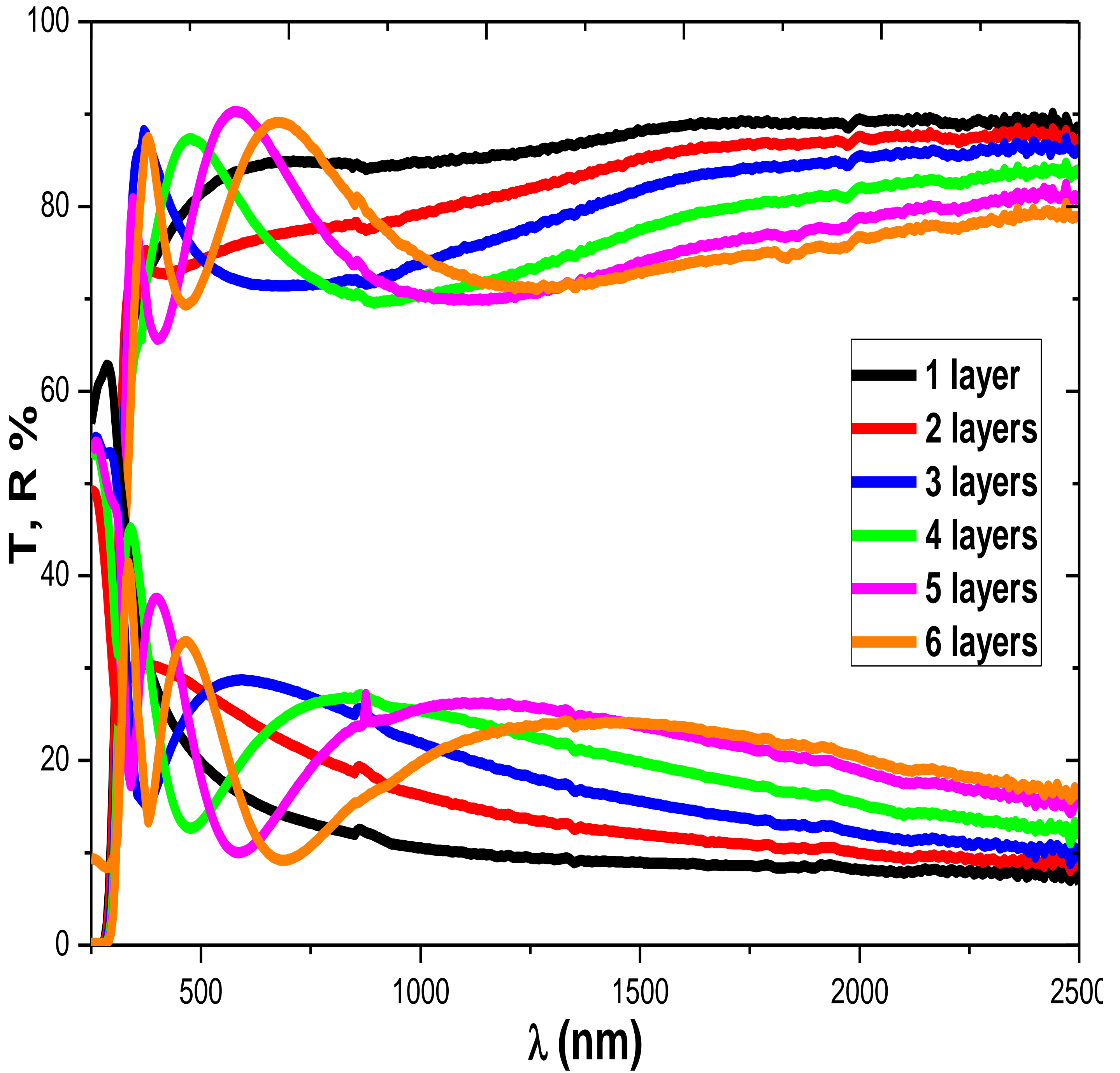

Figure 5

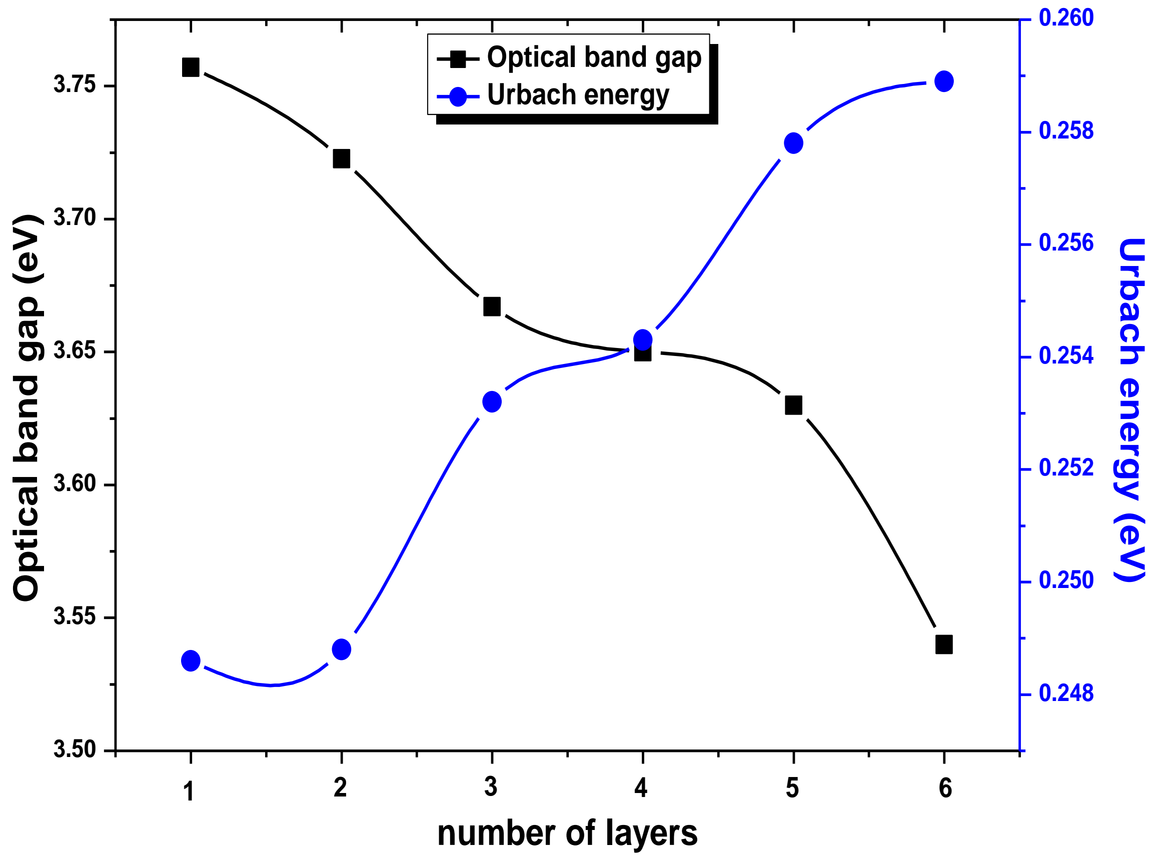

Figure 6

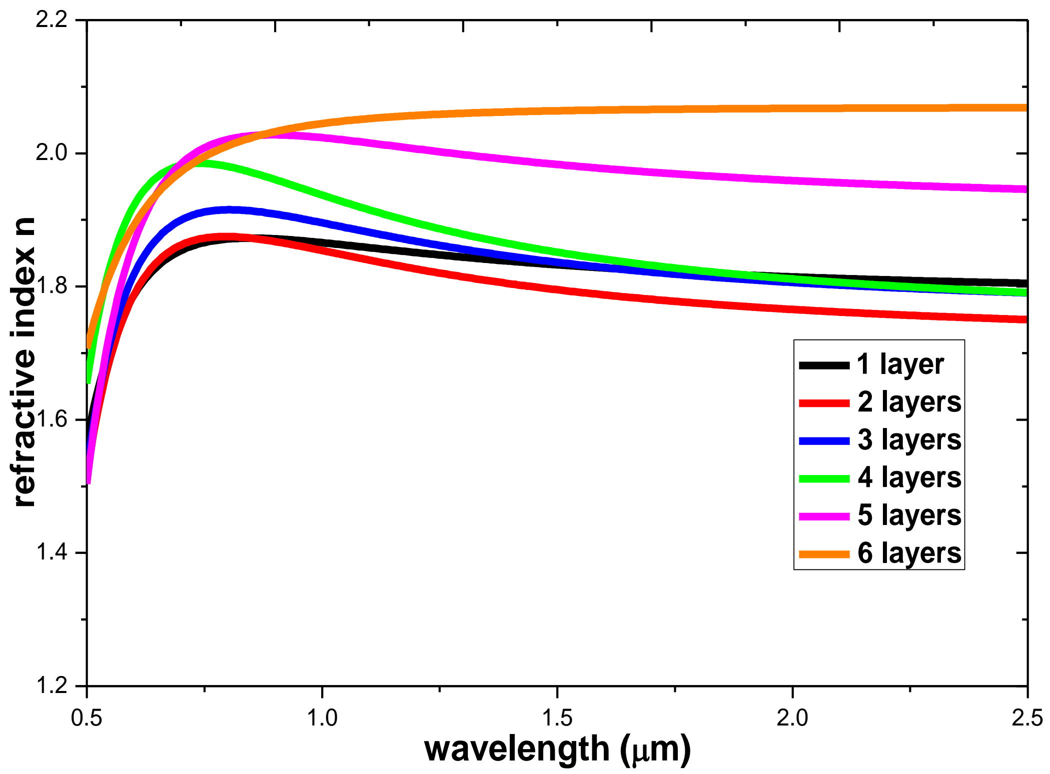

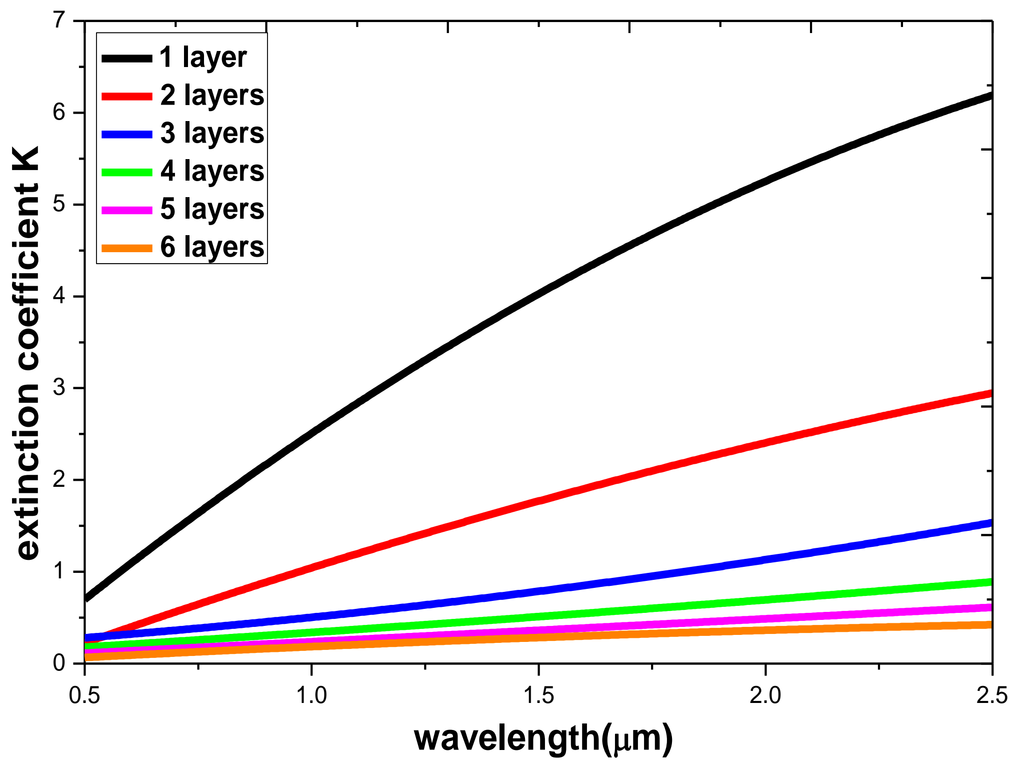

Figure 7

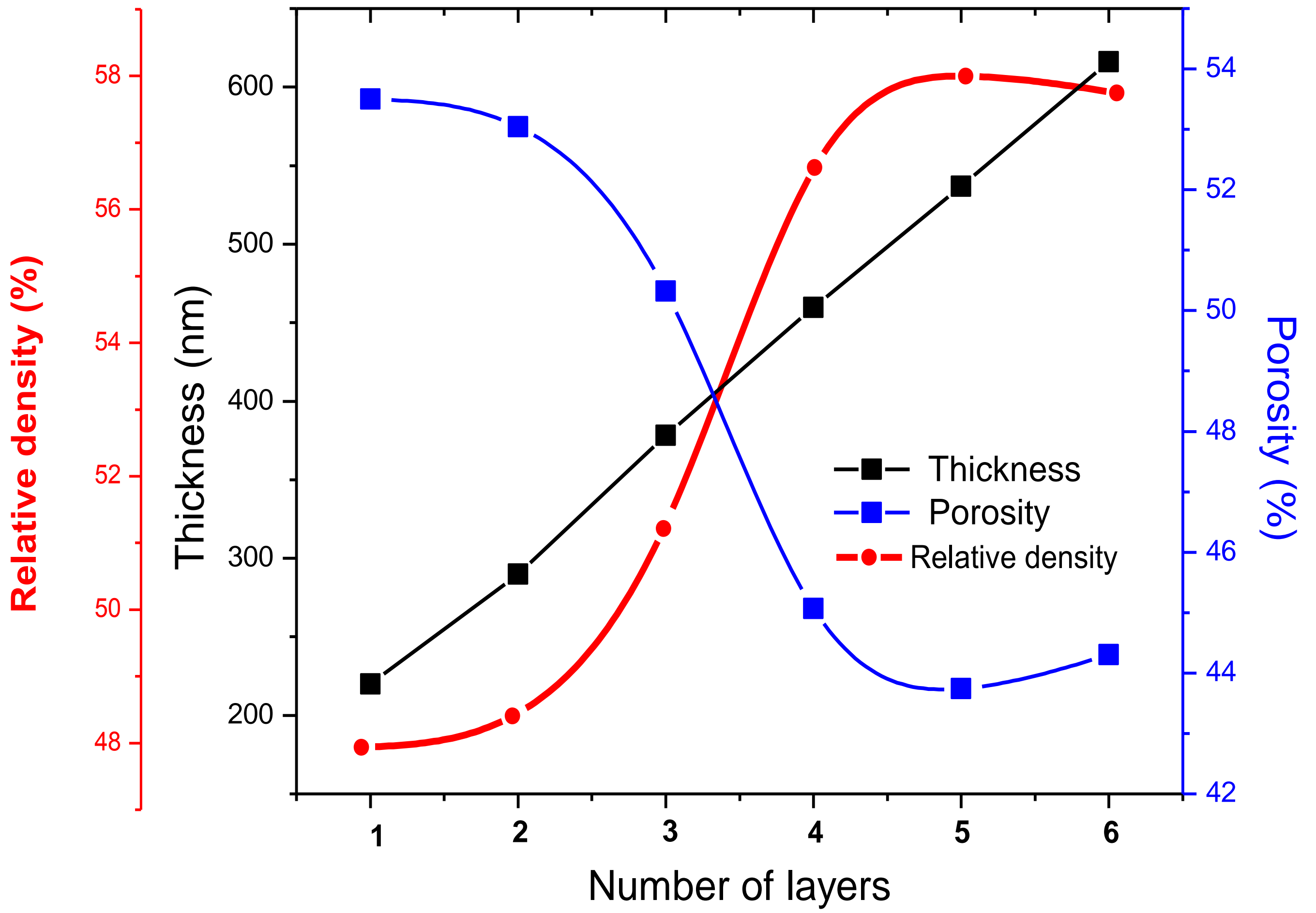

Figure 8